5-1998

Separating Baroclinic Flow From Tidally Induced Flow in Estuaries

Chunyan Li
Old Dominion University

Arnoldo Valle-Levinson
Old Dominion University

Kuo Chuin Wong

Kamazima M. M. Lwiza

Original Publication Citation

Li, C. Y., Valle-Levinson, A., Wong, K. C., & Lwiza, K. M. M. (1998). Separating baroclinic flow from tidally induced flow in estuaries. *Journal of Geophysical Research: Oceans, 103*(C5), 10405-10417. doi:10.1029/98jc00582

JOURNAL OF GEOPHYSICAL RESEARCH, VOL. 103, NO. C5, PAGES 10,405–10,417, MAY 15, 1998

Separating baroclinic flow from tidally induced flow in estuaries

Chunyan Li and Arnoldo Valle-Levinson

Center for Coastal Physical Oceanography, Old Dominion University, Norfolk, Virginia

Kuo Chuin Wong

College of Marine Studies, University of Delaware, Newark

Kamazima M. M. Lwiza

Marine Science Research Center, State University of New York at Stony Brook

Abstract. A simple method is used to separate the tidally induced and density-driven subtidal flows in a coastal plain estuary. This method is applicable to weak wind conditions and to systems with appreciable fortnightly variation of tidal amplitude. The baroclinic density-driven motion is assumed to depend on the river discharge, which generates a horizontal density gradient, and is weakened by vertical mixing, which in turn depends on tidal forcing. The barotropic tidally induced motion is assumed to be a function of the tidal amplitude. By Taylor series expansions, two equations are obtained. These equations show the dependence of the tidally induced flow component on the tidal amplitude and the dependence of the density-driven flow component on the ratio between river discharge and tidal amplitude, respectively. The method is applied to water velocity data obtained in the James River, Virginia, in October-November 1996. The data cover two spring tidal cycles and two neap tidal cycles. The vertical structures, as well as the depth mean, of both tidally induced and density-driven components of the subtidal flow are obtained. Results show that the tidally induced component has a predominant seaward flow in the channel and a landward flow over the shoals. The density-driven exchange flow is seaward over the shoals and landward in the channel. These results are consistent with theoretical model results which show that the tidally induced component and density-driven component compete against each other. The increased tidal mixing and tidally induced exchange flow during spring tides reduce density-driven motion, which results in a weak net subtidal flow. In contrast, during neap tides, both the tidally induced flow component of the subtidal flow and tidal mixing are weak, and the tidally induced flow is overwhelmed by the density-driven flow component, which results in a stronger subtidal flow. By extending the proposed method, we suggest that future studies use a least squares fitting technique to obtain an optimal estimate for the tidally induced and density-driven subtidal flow components.

1. Introduction

Estuarine circulation is produced by horizontal density gradients, tidal forcing, wind stress, river discharge, and coastal sea level fluctuations. Other factors, such as bathymetry and Coriolis force, may also influence the flow. Because of the complexity of the many processes that affect estuarine hydrodynamics, most studies have focused on individual mechanisms. The classical theory of estuarine circulation of *Pritchard* [1952, 1954, 1956] and *Hansen and Rattray* [1965] dealt with baroclinic (gravitational) subtidal flow only. On the other hand, most of the studies on tidally induced subtidal flow have excluded the gravitational flow component to keep the problem mathematically tractable [*Ianniello*, 1977a, b; *Li and O'Donnell*, 1997]. Typical analytical methods solve the individual contributions first and obtain the net result by the summation of the individual contributions [*Jay and Smith*, 1990; *McCarthy*, 1991; *Friedrichs and Hamrick*, 1996]. The objective of this paper, however, is to separate the individual contribu-

Paper number 98JC00582.
0148-0227/98/98JC-00582$09.00

tions to the subtidal flow. Specifically, a simple method is presented to separate the density-driven and tidally induced flows from the subtidal flow signal. In section 2, an overview of previous studies on the tidally induced and density-driven circulation is presented. A method for the separation of the two components is then proposed. Subsequently, an application of this method is demonstrated for an acoustic Doppler current profiler (ADCP) data set obtained in the James River Estuary in the fall of 1996.

2. Background: Tidally Induced Versus Density-Driven Flows

In many estuaries, tidally induced and density-driven flows are the major components of the subtidal flow. The increased need for a better understanding of the transport of waterborne materials in coastal plain estuaries has prompted considerable studies for both two-dimensional and three-dimensional structures of the subtidal flows [*Hamrick*, 1979; *Kjerfve*, 1978, 1986; *Wong*, 1994; *Valle-Levinson and Lwiza*, 1995; *Valle-Levinson and O'Donnell*, 1996; *Friedrichs and Hamrick*, 1996; *Wang and Chao*, 1996; *Li and O'Donnell*, 1997]. Models of rectangular cross sections describe tidally induced mean flow to be landward on the surface and seaward below [*Ianniello*, 1977a, b]. This type of two-layer circulation is the opposite of the gravitational flow of *Pritchard* [1952, 1954, 1956] and *Hansen and Rattray* [1965], which is seaward in the upper layer and landward below.

Studies on models of nonrectangular cross sections [*Hamrick*, 1979; *Wong*, 1994] have shown that a lateral variation of depth causes a lateral variation of turbulence and bottom friction, which results in a tilt of the conventional gravitational flow of *Pritchard* [1952, 1954, 1956] and *Hansen and Rattray* [1965]; that is, the flow pattern changes from one with pure vertical shear to one with lateral shear. Since the horizontal pressure force due to a horizontal density gradient is proportional to the local depth, the tendency of the heavier salty water to replace the lighter freshwater landward is stronger in the channel than over the shoals. The landward flow thus tends to be located in the channel. A seaward flow is required on the shoals because of mass conservation constraint. Observations in lower Delaware Bay [*Wong*, 1994] and lower Chesapeake Bay [*Valle-Levinson and Lwiza*, 1997] have shown this type of subtidal flow.

Interestingly, when the lateral depth variation is taken into account, the two-layer tidally induced mean flow of *Ianniello* [1977a, b] is tilted across the estuary as well. Application of a three-dimensional numerical model developed by *Li and Fang* [1995] demonstrated landward flow over the shoals and seaward flow in the channel [*Li*, 1996]. Numerical model studies applied to the James River Estuary [*Friedrichs and Hamrick*, 1996] and the upper Chesapeake Bay [*Wang and Chao*, 1996; *Galperin and Mellor*, 1990] also showed this type of mean flow. Several two-dimensional (2-D) and three-dimensional (3-D) analytical models and a 2-D numerical model developed by *Li* [1996] presented a systematic study on the effects of the lateral depth variation, which showed similar results. The study suggests that in shallow estuaries of significant lateral depth variation, the mean exchange flow is often as strong laterally as it is vertically.

An extreme case of this type of subtidal flow is when the shoal is so shallow that it becomes a drying sandbank which only experiences the flood phase of the tide. Under this condition, it is easier to understand why the tidally induced net flow over the shoal should be landward [*Bowers and Al-Barakati*, 1997]. A net return flow in the channel is required for mass conservation. Observations have shown that this type of subtidal flow exists in estuaries and shallow seas under much broader conditions. Nearly 4 decades ago, *Robinson* [1960] indicated that in narrow estuaries, there was often a dominant ebb channel. This was further verified by drifter experiments conducted in 1961-1963 in lower Humber Estuary, England [*Robinson*, 1965]. Observations in the Dutch Wadden Sea [*Zimmerman*, 1974], Tay Estuary [*Charlton et al.*, 1975], Mersey Estuary [*Prandle et al.*, 1990], and lower Hudson Estuary [*Lwiza and Connolly*, 1998] also showed similar results.

In a study based on 9 days of observations at North Inlet, South Carolina [*Kjerfve*, 1978], the tidally averaged velocity structure across the inlet was found to be opposite to the gravitational flow suggested by *Fischer* [1972], *Hamrick* [1979], and *Wong* [1994]. The residual flow at North Inlet was shown to be landward at every depth in shallow areas and seaward in the deeper areas of the same cross section. Note that North Inlet is a vertically well-mixed estuary where the salinity is typically 30-35 and the water is very shallow (a few meters) with a relatively large tidal range from 0.9 m on a neap tide to 2.5 m on an extreme spring tide [*Kjerfve*, 1986]. Therefore the tidally induced flow is a major contributor to the mean flow, particularly during spring tides.

In a second field study at North Inlet [*Kjerfve and Proehl*, 1979], data from three consecutive tidal cycles showed a result similar to the first study but with a more detailed structure of the residual velocity profile across the section. The calculated maximum tidal mean velocity reached 0.48 m/s seaward in the channel and 0.21 m/s landward on the shallower side. Although the results of this experiment were consistent with the earlier study [*Kjerfve*, 1978], the difference in magnitudes suggested a dependence on tidal range and coastal far-field forcing, which varied at low frequency. To obtain a more reliable estimate of net exchange flow, another intensive field study was conducted for 32 tidal cycles covering both spring and neap tides in 1979 [*Kjerfve*, 1986]. The results further confirmed the pattern observed previously and showed that the exchange flow averaged over 16 spring tidal cycles was stronger than that averaged over 16 neap tidal cycles (Figure 1), indi-

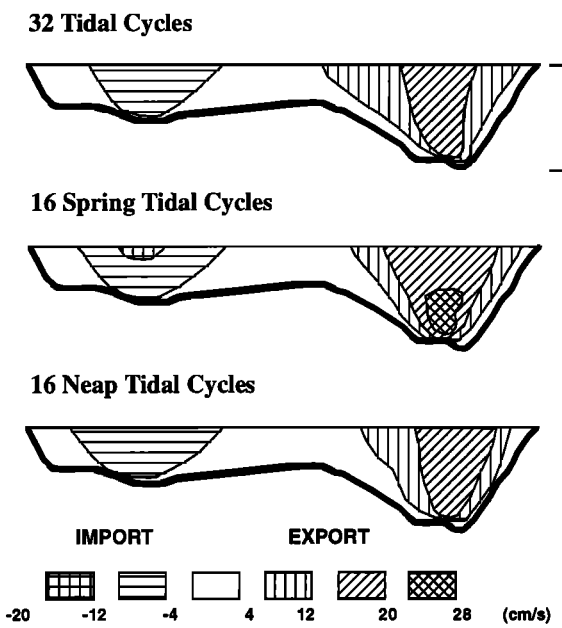

Figure 1. Subtidal flow observed in North Inlet, South Carolina [*Kjerfve*, 1986].

cating that the subtidal circulation was tidally induced. This is clearly in contrast to other observations which showed smaller subtidal flow at spring tides than at neap tides [*Nunes and Lennon*, 1987; *Nunes et al.*, 1989; *Linden and Simpson*, 1988].

Li and O'Donnell [1997] proposed a theory for the tidally induced subtidal exchange flow in a shallow estuary with lateral depth variation. They suggested that the inward flux was mainly due to the surface fluctuation of a progressive or partially progressive tidal wave, which required a seaward residual pressure gradient to drive the water outward for mass to balance. Since the surface elevation in a narrow estuary had only a small lateral variation, the depth-integrated longitudinal pressure force was mainly dependent on the depth, which was greater in the channel than on the shoals. As a result, a larger return flow occurred in the channel than over the shoals. The net effect was a landward flow over the shoals and a seaward flow in the channel. This flow distribution was the opposite to that of a tilted conventional (gravitational) estuarine circulation [*Hamrick*, 1979; *Wong*, 1994].

These theories and observations suggest that the gravitational circulation competes with the tidally induced mean flow regardless of the cross-sectional shape of the estuary. When rectangular cross sections are applicable, the competition is in the vertical plane with seaward flow at the surface and landward flow at the bottom due to gravitational circulation but landward flow at the surface and seaward flow underneath due to tidal nonlinearities. When nonrectangular cross sections are applicable, the competition may turn to the lateral plane with seaward flow over the shoals and landward flow in the channel due to gravitational circulation but landward flow over the shoals and seaward flow in the channel due to tidal nonlinearities.

It is important to note that observations have indicated two contradictory flow patterns: one with increased magnitude of exchange flow [*Kjerfve*, 1986] while the other with decreased magnitude of exchange flow [*Nunes and Lennon*, 1987; *Nunes et al.*, 1989; *Linden and Simpson*, 1988] during spring tides. The first pattern fits the response of a tidally induced system in which an increased tidal motion increases nonlinearities and mean flows [*Ianniello*, 1977a, b; *Li and O'Donnell*, 1997]. Figure 2 shows the maximum tidally induced residual flow in an estuary with a v-shaped cross section as a function of tidal forcing at the mouth [*Li and O'Donnell*, 1997]. As the tidal forcing increases, so does the net flow. The second pattern, in which the net flow decreases in spring tide, has been entirely attributed to the increased vertical mixing during spring tide [*Nunes and Lennon*, 1987; *Nunes et al.*, 1989; *Linden and Simpson*, 1988]. While the increased vertical mixing does reduce stratification and thus weakens baroclinic flow, it is only part of the story. Since the tidally induced subtidal flow tends to oppose the baroclinic subtidal flow, the effect is an additional reduction of total net flow during spring tide in estuaries of sufficient river runoff. This effect has apparently been ignored in previous studies. In section 3, we present a simple method to account for the effects of nonlinear tide and gravitational circulation modulated by the change of tidal mixing due to the change of tidal forcing. By this method, we separate the density-driven flow from the tidally induced flow.

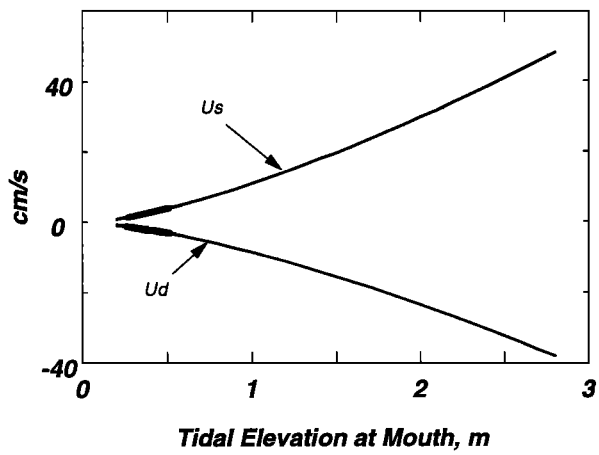

Figure 2. Dependence of tidally induced depth-averaged flow on tidal forcing in an estuary with a v-shaped cross section [from *Li and O'Donnell*, 1997]. The U_s and U_d are the maximum along-channel subtidal velocities over the shoal and in the channel, respectively. The highlighted segments of the curves indicate the range corresponding to the James River.

3. Separating the Tidally Induced Flow From the Gravitational Flow

The circulation in estuaries is nonlinear by nature. The nonlinearities arise from the advection of momentum, finite water elevation, which enters the problem as a surface kinematic boundary condition, and bottom friction [*Parker*, 1991]. These nonlinearities drive the tidally induced circulation [*Ianniello*, 1977a, b] and its interaction with the density-driven circulation. Therefore, in general, the subtidal horizontal velocity u can be expressed as

$$u = u_{bt} + u_{bc} \tag{1}$$

in which u_{bt} is the barotropic component of the subtidal flow in the absence of a density gradient and u_{bc} is the baroclinic component of the subtidal flow, generated by a nonuniform density field. In the following, we will use the terms "barotropic component" and "tidally induced flow" interchangeably. We will also use the terms "baroclinic component" and "density-driven flow" interchangeably. The velocity components in (1) are functions of position. For convenience, we only discuss one component of the horizontal velocity in a Cartesian coordinate. The following formulation also applies to the other Cartesian component. Obviously, because of its nonlinear nature, u_{bc} is not independent of tide.

For simplicity, we only include the tidally induced mean flow in the barotropic component u_{bt}. This, of course, is only applicable to conditions when the tidally induced motion is dominant over other forcings such as the wind. It has been shown that tidally induced mean flow inside the estuary increases with the tidal amplitude at the mouth [*Li and O'Donnell*, 1997]. As shown in Figure 2, the increase of the mean flow with tidal forcing is almost linear, particularly if the variation of the tidal elevation is small (of the order of 1 m or less). For this reason, the following analysis assumes that the barotropic component is proportional to the tidal amplitude at the mouth. This assumption can also be explained by Taylor series expansion. To illustrate this, recall that tidally induced flow is a function of the nonlinear parameter $\epsilon = a/h_0 < 1$ [*Ianniello*, 1977a], where a and h_0 are the tidal amplitude and mean depth, respectively. Therefore

$$u_{bt} = u_{bt}(\epsilon) \tag{2}$$

Taylor series expansion at $\epsilon = 0$ gives

$$\begin{aligned} u_{bt}(\epsilon) &= u_{bt}(0) + \epsilon u_{bt}^{'}(0) + \frac{\epsilon^2}{2} u_{bt}^{''}(0) + \cdots \\ &= u_{bt}(0) + a\beta_1 + a^2\beta_2 + \cdots \end{aligned} \tag{3}$$

in which β_1 and $\beta_2, \cdots$, are constants independent of a and primes denote derivatives. Since the tidally induced net flow is present only if there is tidal input at the mouth ($a \neq 0$), we have $u_{bt}(0) = 0$ and therefore, correct to the first order,

$$u_{bt} = a\beta_1 + \mathcal{O}(\epsilon^2) \tag{4}$$

To incorporate both tidal mixing and river input into the baroclinic component u_{bc}, we postulate that the gravitational flow is a function of α, the ratio between the volume input of freshwater (TR) and the volume input of seawater (aS) into the estuary during one tidal cycle; that is,

$$\alpha = \frac{TR}{aS} \tag{5}$$

and

$$u_{bc} = u_{bc}(\alpha) \tag{6}$$

in which T, R, a, and S are the tidal period (in seconds), river discharge rate (in cubic meters per second), tidal amplitude (in meters), and the surface area (in squared meters) of the estuary within which most of the mixing occurs, respectively. For the James River, a moderate river flow is $R \sim 100\ \mathrm{m}^3/\mathrm{s}$. We choose an average width of 4 km and a length of tidal excursion of 10 km, which yield $S \sim 4 \times 10\ \mathrm{km}^2 = 4 \times 10^7\ \mathrm{m}^2$. If $a \sim 1$ m and $T =$ 12 hours, we have $\alpha \sim 10^{-1} < 1$. Again, using Taylor series expansion,

$$\begin{aligned} u_{bc}(\alpha) &= u_{bc}(0) + \alpha u_{bc}^{'}(0) + \frac{\alpha^2}{2} u_{bc}^{''}(0) + \cdots \\ &= u_{bc}(0) + \frac{R}{a}\alpha_1 + \left(\frac{R}{a}\right)^2 \alpha_2 + \cdots \end{aligned} \tag{7}$$

in which α_1 and $\alpha_2, \cdots$, are independent of R/a. Note that T and S are now absorbed into α_1 and α_2, etc. These α constants are to be determined together with the β constants.

Since the gravitational circulation is present only if river flow is nonzero, we have $u_{bc}(0) = 0$ and therefore

$$u_{bc}(\alpha) = \frac{R}{a}\alpha_1 + \left(\frac{R}{a}\right)^2 \alpha_2 + \cdots \tag{8}$$

Correct to the first order,

$$u_{bc}(\alpha) = \frac{R}{a}\alpha_1 + \mathcal{O}(\alpha^2) \tag{9}$$

The theoretical model of *Hansen and Rattray* [1965] shows that an increase of vertical eddy viscosity reduces the gravitational flow, which has been demonstrated by experiments [*Linden and Simpson*, 1988] and observed in estuaries [*Peters*, 1997]. In addition, according to an empirical relationship of *Bowden* [1967] and a theoretical result of *Ianniello* [1977a], the eddy viscosity is proportional to the amplitude of the tidal velocity, which in turn is proportional to the amplitude of tidal elevation. A larger tidal forcing therefore causes more intense mixing, which in turn reduces the gravitational flow. This feature is represented in the inverse proportionality of u_{bc} to a in (8) or (9). A similar relationship was suggested by *Godfrey* [1980] for the James River Estuary. Therefore (8) and (9) are consistent with these

theories and observations. We caution, however, that (8) and (9) may be limited to weak or moderate river discharge. For very large river discharges ($\sim 10^3$ m^3/s, when $\alpha \sim 1$ for the James River Estuary), the Taylor series expansion may not be valid. Under this condition, the water inside the estuary can be completely fresh, and the mixing of freshwater and saltwater, as well as the baroclinic motion, may actually occur outside the estuary.

On the bases of (4) and (9), appropriate experiments can be designed to measure the current profiles in a shallow estuary of significant fortnightly tidal amplitude variation and to separate the barotropic and baroclinic components. First, the current is measured at chosen positions or transect(s) encompassing a spring tide and a neap tide. Harmonic analysis is then performed to calculate the subtidal current and the amplitude and phase of the semidiurnal and diurnal tidal currents for both spring and neap periods. Two equations are obtained for each measurement location which are sufficient to solve the constants α_1 and β_1 and thus the barotropic and baroclinic components. Mathematically,

$$u^{(s)} = u_{bt}^{(s)} + u_{bc}^{(s)} \tag{10}$$

$$u^{(n)} = u_{bt}^{(n)} + u_{bc}^{(n)} \tag{11}$$

in which the superscripts s and n indicate spring tide and neap tide, respectively. From (4) and (9), we have, dropping the subscript 1 for clarity,

$$u_{bt}^{(s)} = \beta a^{(s)} \tag{12}$$

$$u_{bc}^{(s)} = \alpha \frac{R^{(s)}}{a^{(s)}} \tag{13}$$

$$u_{bt}^{(n)} = \beta a^{(n)} = u_{bt}^{(s)} \frac{a^{(n)}}{a^{(s)}} \tag{14}$$

$$u_{bc}^{(n)} = \alpha \frac{R^{(n)}}{a^{(n)}} = u_{bc}^{(s)} \phi \tag{15}$$

where

$$\phi = \frac{R^{(n)}}{R^{(s)}} \Big/ \frac{a^{(n)}}{a^{(s)}} \tag{16}$$

Combining (11), (14), and (15), it follows that

$$u^{(n)} = u_{bt}^{(s)} \frac{a^{(n)}}{a^{(s)}} + u_{bc}^{(s)} \phi \tag{17}$$

Multiplying (10) by ϕ,

$$\phi u^{(s)} = \phi u_{bt}^{(s)} + \phi u_{bc}^{(s)} \tag{18}$$

and then subtracting (18) from (17), the spring tide barotropic component of the subtidal flow can be written as, according to (10),

$$u_{bt}^{(s)} = \frac{\phi u^{(s)} - u^{(n)}}{\phi - a^{(n)}/a^{(s)}} \tag{19}$$

and the baroclinic component at spring tide is

$$u_{bc}^{(s)} = u^{(s)} - u_{bt}^{(s)} = \frac{u^{(n)} - u^{(s)} a^{(n)}/a^{(s)}}{\phi - a^{(n)}/a^{(s)}} \tag{20}$$

In (19) and (20), $a^{(n)}/a^{(s)}$ is the ratio of tidal amplitudes between neap and spring tides. The parameter ϕ is calculated from (16). The calculation of the left-hand side of (19) and (20) is therefore straightforward. This method is now applied to a series of current profiles obtained in the James River Estuary.

4. Application of the Method to Observations

Acoustic Doppler current profiler (ADCP) data from two 25-hour cruises were obtained at the James River Estuary during spring tides (October 26-27, 1996) and neap tides (November 2-3, 1996). Two transects were sampled repeatedly during each cruise (Figure 3). The lengths of the transects were $\sim$ 4 km. The northern side of the transects was deeper with a depth of 12-14 m. The shoals on the southern side were 2-4 m deep. The lateral variation of depth was therefore much larger than the tidal amplitude (of the order of 0.5 m for the spring tide and 0.25 m for the neap tide). A harmonic analysis was performed on the current velocity observations to obtain the semidiurnal and diurnal tidal constituents and the subtidal current. The tidal constituents and subtidal currents were obtained as functions of the horizontal position along the transect and the vertical position. This analysis yielded root-mean-square errors lower than 0.1 m/s throughout the domain sampled. The method proposed in section 3 was then applied to the subtidal component.

The near-surface subtidal current, the near-bottom subtidal current, and the depth-averaged subtidal current for two spring tidal periods (October 26-27, 1996) and two subsequent neap tidal periods (November 2-3, 1996) along the two transects are shown in Figures 4 and 5. The near-surface current is defined at $\sim$ 2.5 m below the surface, and the near-bottom current is defined at a depth of $\sim$ 85% of the water column, below which the ADCP sidelobe effects deteriorate the quality of the data. The tidal range was $\sim$ 0.95 m during the spring tides and 0.49 m during the neap tides. These tidal range values yield $a^{(n)}/a^{(s)} = 0.52$. However, both the near-surface and near-bottom subtidal currents of the neap tides were higher than those of the spring tides (compare Figure 4a with Figure 5a and Figure 4b with Figure 5b) along most of the transects. The near-bottom subtidal current was weak for both spring tides and neap tides (Figure 4b and Figure 5b), less than half of that at the surface. The depth-averaged subtidal current during the neap tides (Figure 5c) was about twice as large as that of the spring tides (Figure 4c). During the neap tides, the landward flow occurred in the deep channel, and seaward flow occurred

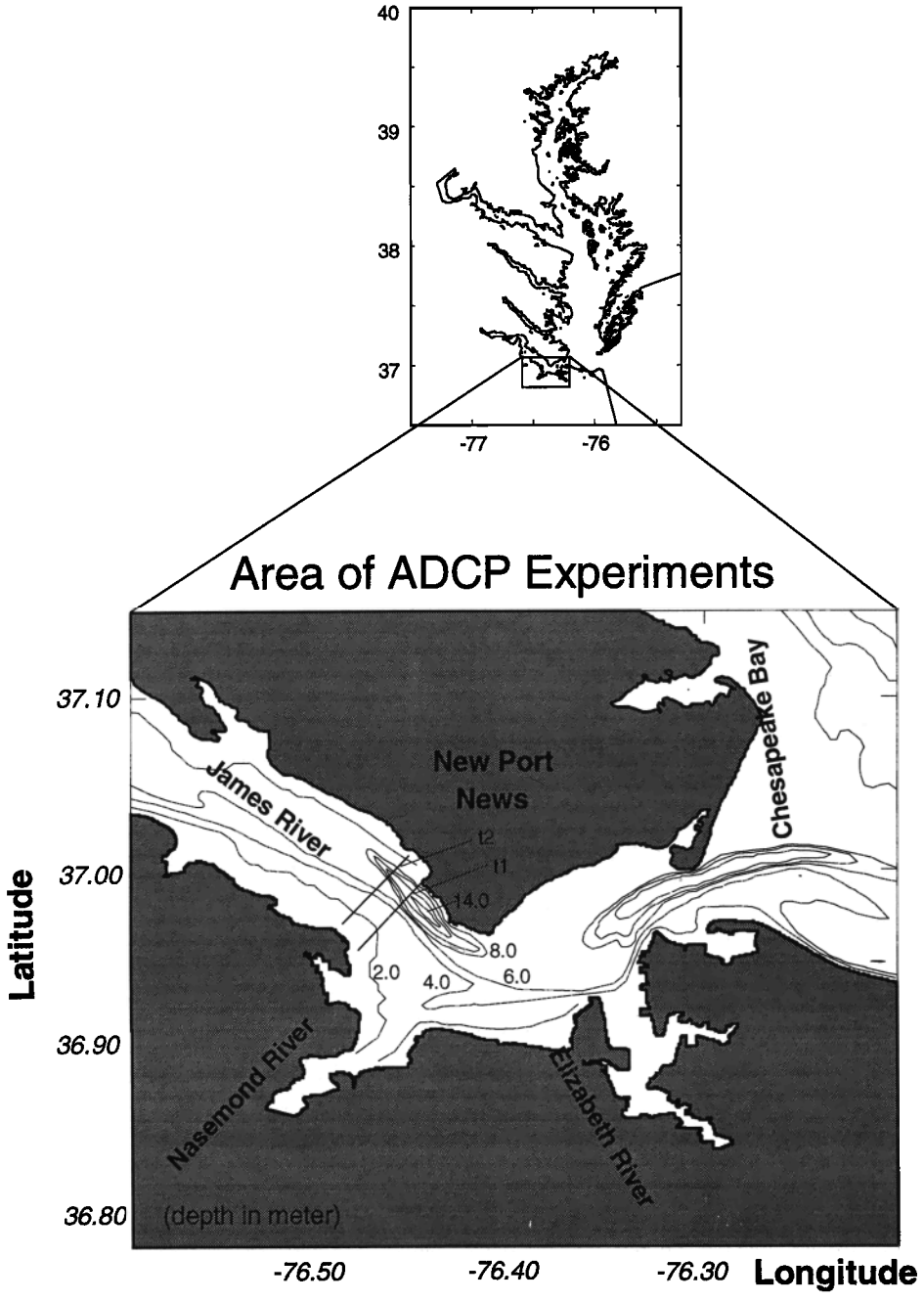

Figure 3. The study area: James River Estuary. The two transects of sampling are shown by the solid straight lines and are denoted by t1 and t2, respectively. Depth contours are in meters.

over the shoals (Figure 5). Since during the neap tides, tidal motion was at a minimum, the result reflected the dominant effect of the baroclinic component. During the spring tides, there was a weak surface inflow both in the deep channel and over the shoal of the upstream transect and a weak surface outflow both in the deep channel and over the shoal of the downstream transect (Figure 4a). There was an outflow between the 4- and 10-m depth contours on both transects. Also, during the spring tide, the near-bottom subtidal flow showed a weak landward flow almost everywhere along the two transects (Figure 4b). The depth-averaged flow during the spring tide showed weak alternating landward and seaward flows along both transects. This indicated that the subtidal flow during the spring tide was weaker and less well defined than the neap tide.

The river discharge before and during the first cruise (October 26-27) was moderate with a mean around 125 m^3/s (Table 1), which was equivalent to $\sim$ 5 mm/s at the transects of the experiment. It decreased by half in the second cruise (November 2-3). By examining data relating an increase of freshwater discharge to a subsequent drop in low-pass-filtered salinity in the James River, we found a delay of $\sim$ 3 days. Therefore, to ob-

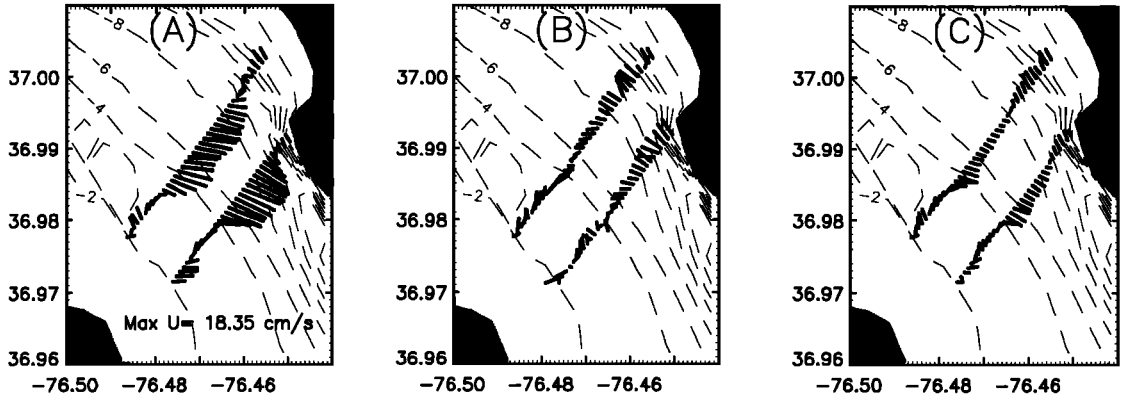

Figure 4. Subtidal current during a spring tide (October 26-27, 1996), including (a) near-surface current, (b) near-bottom current (defined at the depth of 85% of the water column), and (c) depth-averaged subtidal current.

tain the value for ϕ, we chose the average discharge of October 23-24 for $R^{(s)}$ and the average discharge of October 30-31 for $R^{(n)}$, which yielded $R^{(n)}/R^{(s)} = 0.81$. The parameter ϕ is then 1.56.

By applying the method proposed in section 3, the near-surface, near-bottom, and depth-averaged velocity fields for the barotropic component of the subtidal current were determined for the spring tides (Figure 6) and for the neap tides (Figure 7). The flow in Figure 7 is a factor of $a^{(n)}/a^{(s)}$ (0.52 in our case) of that in Figure 6. The baroclinic component for the spring tide was estimated according to (20) (Figure 8). The baroclinic component for the neap tide was a factor of ϕ (1.56 in our case) of that for the spring tide. The near-surface barotropic component and the near-surface baroclinic component during the spring tide had maxima of 0.20 and 0.14 m/s, respectively (Figures 6a and 8a). The depth-averaged barotropic component (Figure 6c) and baroclinic component (Figure 8c) during the spring tide had magnitudes of $\sim$ 0.15 and 0.12 m/s, respectively, about twice as large as the total net flow during the spring tide.

An important feature of the results was that both the barotropic and baroclinic components had lateral structures that were clearly correlated with the bathymetry. The barotropic component was seaward in the deep channel and landward over the shoals (Figure 6), while the baroclinic component was landward in the channel and seaward over the shoals (Figure 8). During the spring tides, the barotropic component was strong enough to cancel the effect of the baroclinic component, which resulted in a weak depth-averaged subtidal current (Figure 4c). During the neap tides, the barotropic component (Figure 7) was much weaker than the baroclinic component (1.56 times the magnitude of that shown in Figure 8), which resulted in a depth-averaged subtidal current (Figure 5c) that was stronger than that of the spring tides (Figure 4c) and that had a structure similar to that of the baroclinic component (Figure 8).

For the baroclinic component, the near-bottom current was in the opposite direction to the near-surface current in the middle of the transects between the 4- and 8-m depth contours (compare Figure 8a with Fig-

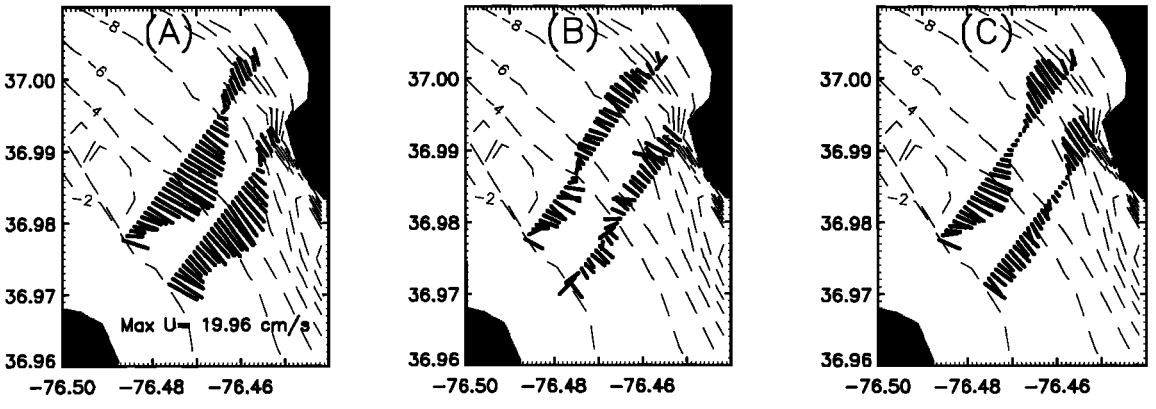

Figure 5. Subtidal current during a neap tide (November 2-3, 1996), including (a) near-surface current, (b) near-bottom current (defined at the depth of 85% of the water column), and (c) depth-averaged subtidal current.

Table 1. James River Discharge

Discharge, ft^3/s	Discharge, m^3/s	Date 1996
4670	132	Oct. 22
4620	131	Oct. 23
4550	129	Oct. 24
4450	126	Oct. 25
4340	123	Oct. 26*
4240	120	Oct. 27*
4070	115	Oct. 28
3840	109	Oct. 29
3740	106	Oct. 30
3680	104	Oct. 31
1890	54	Nov. 1
2100	59	Nov. 2*
1970	56	Nov. 3*

*Date of Doppler current profiler observations.

ure 8b). The change in direction of the near-surface subtidal current for the baroclinic component occurred near the 8-m depth contour in the middle of the transects (Figures 6a, 7a, and 8a). In contrast, the change in direction of the near-bottom subtidal current for both components occurred near the 4-m depth contour on the shoals of the transects (Figures 8b). As a result, the depth-averaged values for the baroclinic component were close to zero in the middle of the transects between the 4- and 8-m depth contours (Figure 8c). The depth-averaged exchange flows were thus quite different in the channel with respect to the shoals.

The vertical structure of the along-channel subtidal currents in both spring and neap tides and the barotropic and baroclinic components during the spring tides are shown in Figures 9-12. The subtidal currents during both experiments (for the spring and neap tides) had a subsurface maximum in the channel and a surface maximum flowing in the opposite direction over the shallower side. During the spring tides, the subsurface maximum over the channel was centered at about 7-9 m depth (Figures 9a and 9b), while the surface current was above 4 m and was located between 2 and 3.5 km along transect 1 or the downstream transect (Figure 9a) and between 1 and 3 km along transect 2 or the upstream transect (Figure 9b). During the neap tides, the subsurface maximum over the channel was centered at ~ 5-6 m depth for both transects (Figures 10a and 10b), while the surface maximum was above 4 m and was located between 0.5 and 3.3 km along transect 1 (Figure 10a) and between 0.5 and 2.9 km along transect 2 (Figure 10b). The strength of both the surface and subsurface currents was greater during the neap tides than during the spring tides (compare Figure 9 with Figure 10).

The barotropic and baroclinic components also exhibited a well-defined surface current over the shoal and subsurface maximum in the channel (Figures 11 and 12), with comparable magnitudes relative to those of the subtidal currents (Figures 9 and 10). The surface current of the baroclinic component seemed to extend closer to the channel from 0 to ~ 3 km along both transects (Figures 12a and 12b), compared to that of the barotropic component, which only extended to about 2-2.5 km (Figures 11a and 11b). In part of the transects, the surface flow and the bottom flow were in opposite directions. For the barotropic component, this region was from 2 to 2.2 km for transect 1 (Figure 11a) and from 1.5 to ~ 2.5 km for transect 2 (Figure 11b). For the baroclinic component, this region was larger: from 1.9 to 3.2 km for transect 1 (Figure 12a) and from 1.5 to ~ 2.9 km for transect 2 (Figure 12b). The characteristics of the baroclinic flow resemble the results of *Hamrick* [1979] and *Wong* [1994] for partially mixed and well-mixed estuaries. The well-defined cores of landward flow in Figure 12 were similar to those predicted by *Wong* [1994].

5. Discussion

The application of our method to the James River Estuary showed that the baroclinic component of the

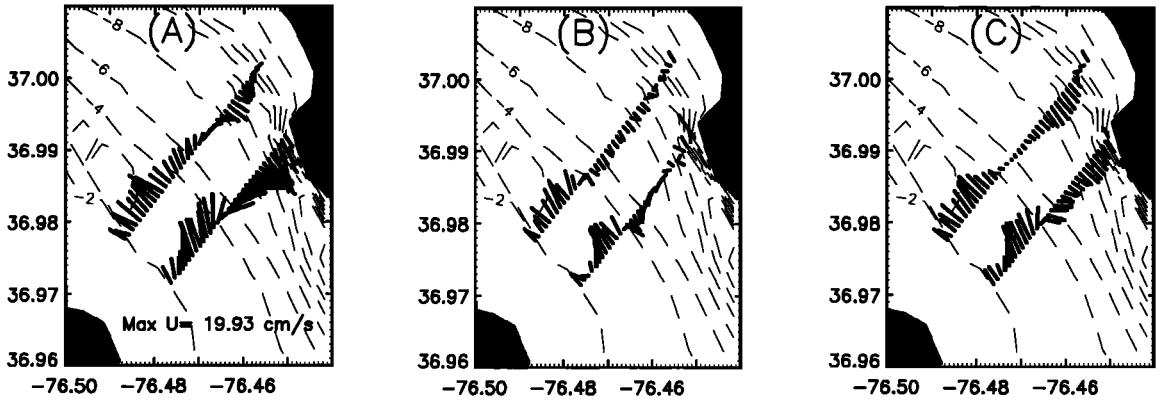

Figure 6. Barotropic component of the subtidal current during the spring tide, including (a) near-surface current, (b) near-bottom current (defined at the depth of 85% of the water column), and (c) depth-averaged current.

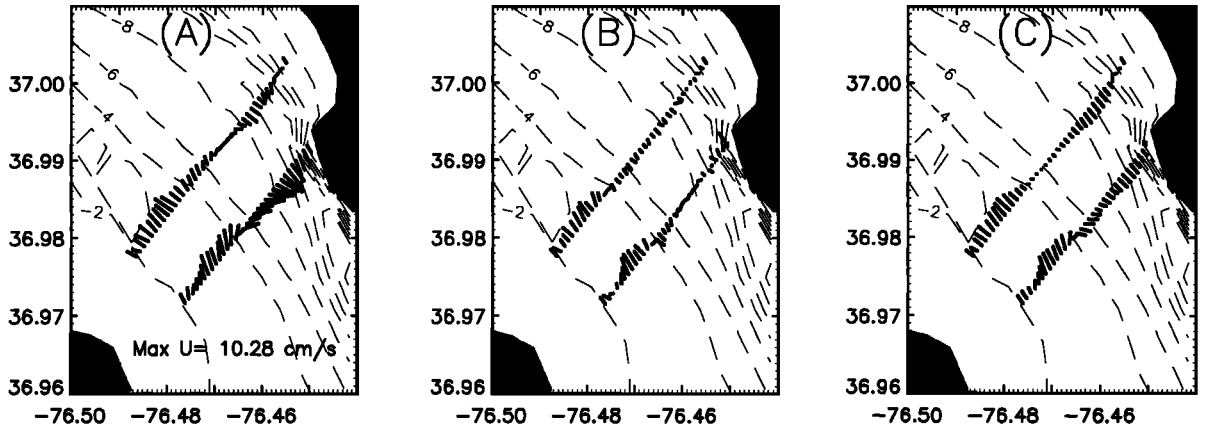

Figure 7. Barotropic component of the subtidal current during the neap tide, including (a) near-surface current, (b) near-bottom current (defined at the depth of 85% of the water column), and (c) depth-averaged current.

subtidal current opposed the tidally induced mean flow. The latter had about the same magnitude as the former during the spring tide. This, of course, was true for the given conditions of river discharge and tidal amplitude. For a smaller river discharge, the tidally induced mean flow may be more important, and vice versa. Nonetheless, the competition between the two components was consistent with the concepts discussed in section 2. This competition varied with the tidal amplitude in a fortnightly cycle. Previous studies [*Nunes and Lennon*, 1987; *Nunes et al.*, 1989; *Linden and Simpson*, 1988] suggested a spring-neap modulation of the subtidal current due to the variation of the strength of the turbulence arising from tidal mixing. In those studies, the effect of the turbulence in suppressing the subtidal flow was emphasized, and the tidally induced mean flow was ignored. In contrast, the present study incorporated the influence of both river runoff and tidal mixing. Our study confirmed that the reduced subtidal motion resulting from increased tidal amplitude could be attributed not only to the effect of mixing but also to the increase of an apparent current opposing the gravitational flow. It should be noted, however, that the James River Estuary, like many other estuaries, has complicated lateral boundaries that are absent in the theoretical models [*Ianniello*, 1977a, b; *Hamrick*, 1979; *Wong*, 1994; *Li*, 1996; *Li and O'Donnell*, 1997]. More studies are obviously needed along the same transects and elsewhere to investigate the effect of the variation of lateral boundaries.

Because of its simplicity, the method presented here may be easily applied to other shallow estuaries to obtain first-order results of the tidally induced and density-driven flows if the river discharge is moderate and wind is weak. The applicability of this method to other tidal and river discharge regimes shall be explored as more data become available.

In section 3, the barotropic and baroclinic components were obtained without calculating α and β. The parameters can be obtained with the following equations:

$$\alpha = \frac{a^{(s)}u^{(n)} - u^{(s)}a^{(n)}}{R^{(s)}(\phi - a^{(n)}/a^{(s)})} \tag{21}$$

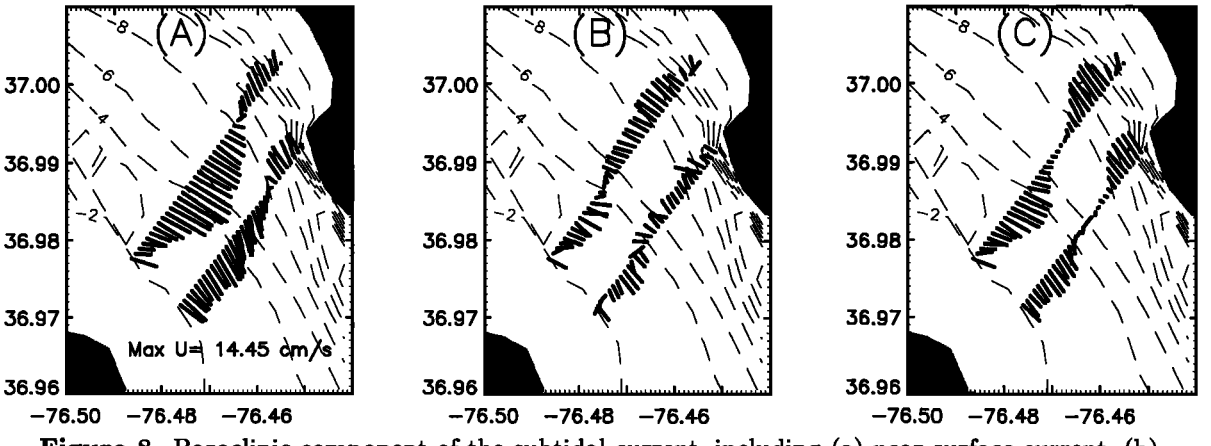

Figure 8. Baroclinic component of the subtidal current, including (a) near-surface current, (b) near-bottom current (defined at the depth of 85% of the water column), and (c) depth-averaged current.

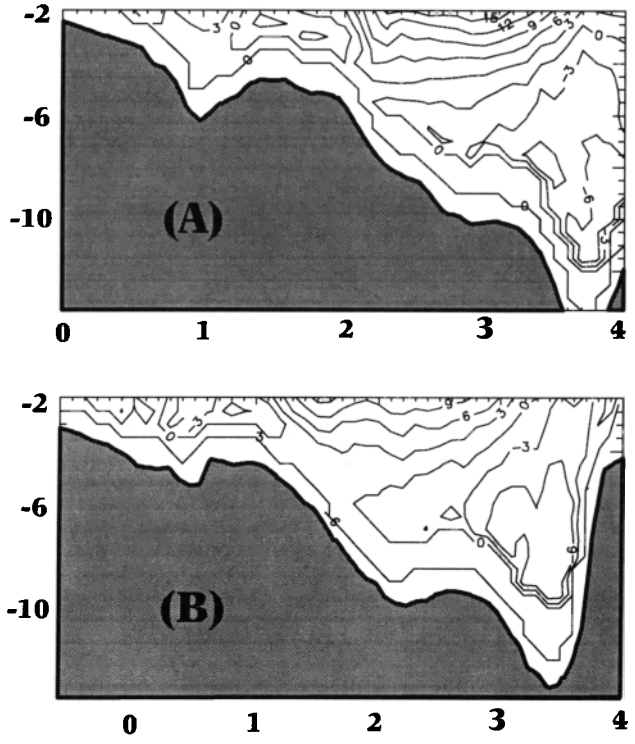

Figure 9. The vertical structure of the along-channel subtidal flow during the spring tide for (a) transect 1 and (b) transect 2.

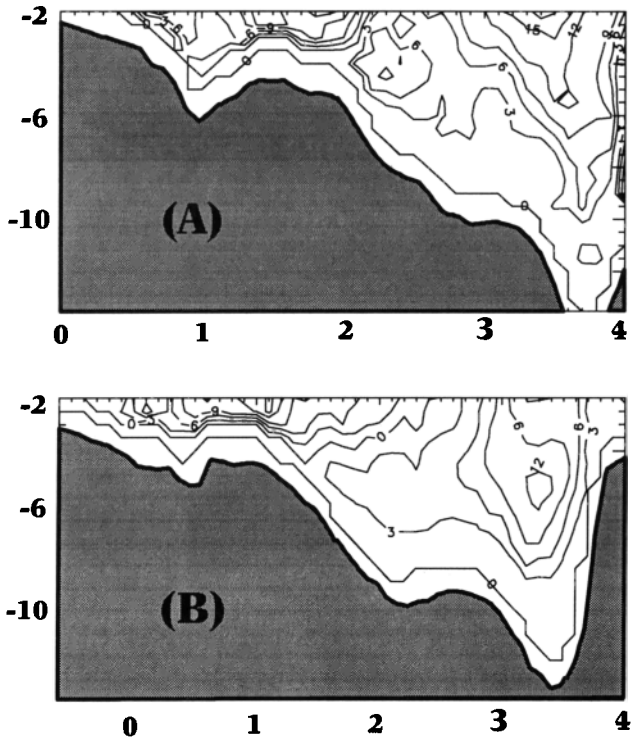

Figure 11. The vertical structure of the along-channel barotropic component of the subtidal flow during the spring tide for (a) transect 1 and (b) transect 2.

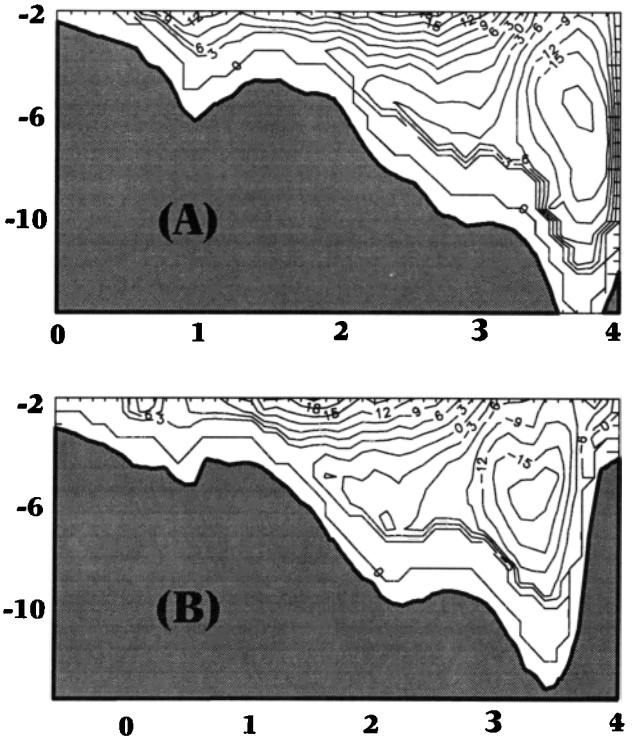

Figure 10. The vertical structure of the along-channel subtidal flow during the neap tide for (a) transect 1 and (b) transect 2.

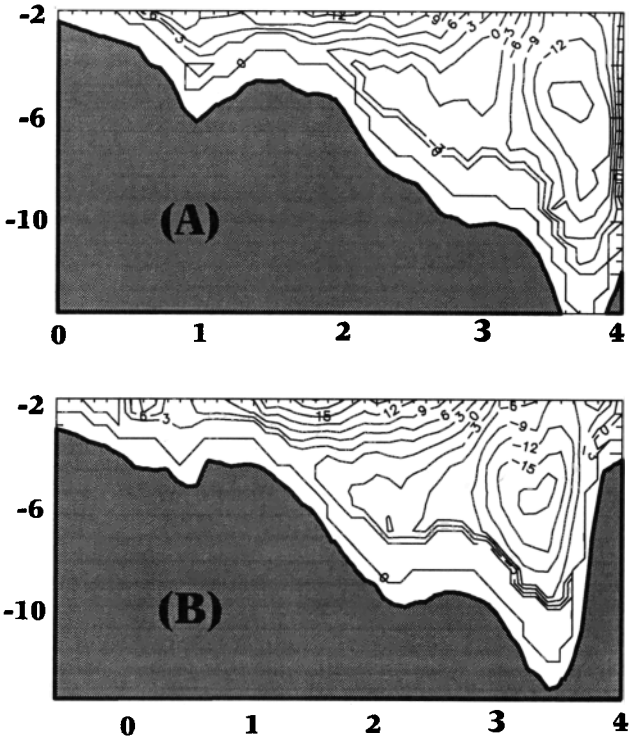

Figure 12. The vertical structure of the along-channel baroclinic component of the subtidal flow during the spring tide for (a) transect 1 and (b) transect 2.

$$\beta = \frac{\phi u^{(s)} - u^{(n)}}{\phi a^{(s)} - a^{(n)}} \tag{22}$$

which are functions of position.

Obviously, the proposed method requires that the denominators of (19)-(22) are not zero. This means that (10) and (11) must be independent of each other. If, during two experiments, the river flows and tidal amplitudes (the input parameters) are identical, then the denominators of (19)-(22) are zero and there is not enough information to determine α and β. If the values of the input parameters are similar during the two experiments, the estimated α and β, therefore the separated components, will have large uncertainties. Theoretically, once α and β are obtained, the subtidal flow can be determined for a given river discharge R and tidal forcing (represented by a) by

$$u = \frac{R}{a}\alpha + a\beta \tag{23}$$

This formula can be considered an expression in terms of two base functions,

$$f_1(a, R) = \frac{R}{a}, \qquad f_2(a, R) = a \tag{24}$$

in which R and a are independent variables as before.

In our study, two observations were used to determine the two unknowns α and β. Generally, we can apply more observations to (23) and use least squares fit to obtain an optimal estimate of α and β. Supposing there are $N(\gg 1)$ observations, it can be shown that the best fit yields

$$\alpha = \frac{2\sum_{i=1}^{N} R_i \sum_{i=1}^{N} u_i a_i - 2\sum_{i=1}^{N} a_i^2 \sum_{i=1}^{N} u_i R_i/a_i}{\left(\sum_{i=1}^{N} R_i\right)^2 - \sum_{i=1}^{N} (R_i/a_i)^2 \sum_{i=1}^{N} a_i^2}$$

$$\beta = \frac{2\sum_{i=1}^{N} R_i \sum_{i=1}^{N} u_i R_i/a_i - 2\sum_{i=1}^{N} (R_i/a_i)^2 \sum_{i=1}^{N} u_i a_i}{\left(\sum_{i=1}^{N} R_i\right)^2 - \sum_{i=1}^{N} (R_i/a_i)^2 \sum_{i=1}^{N} a_i^2} \tag{25}$$

Recalling Taylor series expansion of section 3, we can further extend this method to include more base functions (see Appendix).

In the future, as more observations are acquired in estuaries, this extended method can be implemented and tested. Obviously, different sets of base functions other than those suggested in (24) and in the Appendix can be experimented. This method is rather generic and should be applicable to many estuaries except when the river runoff is too large for gravitational flow to develop inside the estuary, when the wind is dominant over tidally induced flow and gravitational circulation, or when both the spring-neap variability in tidal forcing and the river discharge variability are small. Future studies on this subject should include high-resolution numerical models as the simple method proposed here is not based on a rigorous consideration of dynamics. It is worth mentioning that since (8) is based on the assumption that $u_{bc}(\alpha = 0) = 0$, it implies that the system has reached certain equilibrium. In general, the response of the density gradient to the change of river flow takes some time. If the river discharge approaches zero, a finite density gradient may still exist for a certain period of time and $u_{bc}(0)$ will be nonzero. Therefore, for near-zero discharge, the expansion (7)-(9) may have larger relative errors during a transient period. Practically, the smoother the river discharge variation, the better the approximation of (7)-(9) should be. An alternative of using the river discharge to express the baroclinic flow is using the horizontal density (or salinity) gradient, which should be able to eliminate the limitation of the method presented here. That, however, requires hydrographic data along the estuary. Future studies may compare the two methods, which may provide insight to the dynamics such as how the baroclinic flow will be affected by the variation of river flow. This method is likely to be invalid in regions of high spatial derivatives such as in a strong frontal area [*O'Donnell*, 1993]. Therefore it may not be applicable to salt-wedge estuaries or fjords.

6. Summary

A simple method was introduced to separate the barotropic and baroclinic components of the subtidal current observed in a coastal plain estuary. The method is valid under these conditions: (1) the baroclinic component is a function of both the river discharge and tidal forcing, (2) the barotropic component is proportional to the tidal amplitude at the mouth, and (3) the effect of the wind is smaller than either component. The application of this method to the James River Estuary produced results consistent with known theories and observations. The results showed that both the barotropic and baroclinic components were highly dependent on the lateral variation of the water depth. The subtidal current showed seaward flow over the channel for the barotropic component and seaward flow over the shoal for the baroclinic component. The landward flow was over the shoal for the barotropic component and over the channel for the baroclinic component. The maximum of the subtidal flow over the shoal was at the surface, and the maximum of the subtidal flow in the channel was below the surface. For both barotropic and baroclinic components, there was a surface maximum over the shoal and a subsurface maximum in the channel. This was particularly clear for the baroclinic component, a pattern predicted by *Wong* [1994] with a conceptual model of partially and well-mixed estuaries. In the James River Estuary, for the period studied, the barotropic component during spring tides had a similar

order of magnitude as that of the baroclinic component. Since the two components had opposite patterns of exchange flows, the total subtidal flow during the spring tide was smaller than that during the neap tide. Because the subtidal current during the spring tide was a result of the difference of two functions of similar magnitude, the correlation of the subtidal current with the bathymetry was not well established. In contrast, the subtidal current during the neap tides had a clearer correlation with the bathymetry and resembled the pattern of the baroclinic flow since the barotropic component was at its minimum.

The proposed method is applicable to estuaries where the residual circulation is controlled primarily by tidally rectified current and gravitational circulation. Without modification, it may not work in estuaries where the residual circulation is dominated by wind-driven circulation.

Appendix: Generalization of the Method

To further generalize the method, we can choose more base functions $f_i(a, R)$, for instance,

$$f_1 = a,\ f_2 = a^2,\ \cdots,\ f_M = a^M;$$
$$f_{M+1} = \frac{R}{a},\ f_{M+2} = \left(\frac{R}{a}\right)^2,\ \cdots, f_{2M} = \left(\frac{R}{a}\right)^M \tag{A1}$$

to represent the subtidal flow as

$$u = \sum_{j=1}^{M} f_j \alpha_j \tag{A2}$$

where

$$\begin{aligned} &\alpha_j = \alpha_j, \quad j = 1, 2, \cdots, M \\ &\alpha_j = \beta_{j-M}, \quad j = M+1, M+2, \cdots, 2M \end{aligned} \tag{A3}$$

These base functions are chosen according to the Taylor series expansion. The N observations thus yield

$$u_i = \sum_{j=1}^{M} f_{ji} \alpha_j, \qquad i = 1, 2, \cdots, N \tag{A4}$$

in which $f_{ji} = f_j(a_i, R_i)$. In matrix form this is

$$U = Ax \tag{A5}$$

where $U = (u_1, u_2, \cdots, u_N)^T$, $x = (\alpha_1, \alpha_2, \cdots, \alpha_{2M})^T$, and $A = (f_{ji})$, a $N \times M$ matrix.

By minimizing the error,

$$\delta^T \delta = (U - Ax)^T (U - Ax) \tag{A6}$$

it is easy to show that the best fit is

$$x = (A^T A)^{-1} A^T U \tag{A7}$$

Acknowledgments. This project was funded by U.S. National Science Foundation (NSF Project OCE-9529806, OCE-9530394, and OCE-9530395) and supported by the Center for Coastal Physical Oceanography (CCPO), Department of Oceanography, Old Dominion University. Dozens of faculty members, staff, and students from CCPO, State University of New York, and University of Delaware participated in the field work, and their help was invaluable. The assistance on the field of R. Bray, R.C. Kidd, and W. Check is greatly appreciated. We thank R. K. White of USGS for providing us with the James River discharge data. We thank J. H. Simpson for his review comments which motivated us to use an improved and more general approach. We are grateful to L. P. Atkinson and an anonymous reviewer for their comments, which helped the improvement of the manuscript. C. Li would like to thank B. Lipphardt and C. Lascara for their generous help for the use of the IDL software package for this study. Animations of the data presented here can be found in the following homepage: http://www.ccpo.odu.edu/~arnoldo/transcope/transcope.html.

References

Bowden, K. F., Stability effects on turbulent mixing in tidal currents, *Phys. Fluids Suppl., 10*, S278-S280, 1967.

Bowers, D. G., and A. Al-Barakati, Tidal rectification on drying estuarine sandbanks, *Estuaries, 20*, 559-568, 1997.

Charlton, J. A., W. McNicoll, and J. R. West, Tidal and freshwater induced circulation in the Tay Estuary, *Proc. R. Soc. Edinburgh, Sect. B: Biol., 75*, 11-27, 1975.

Fischer, H. B., Mass transport mechanisms in partially stratified estuaries, *J. Fluid Mech., 53*, 671-687, 1972.

Friedrichs, C. T., and J. M. Hamrick, Effects of channel geometry on cross sectional variations in along channel velocity in partially stratified estuaries, in *Buoyancy Effects on Coastal and Estuarine Dynamics, Coastal Estuarine Stud.*, vol. 53, edited by D. G. Aubrey and C. T. Friedrichs, pp. 283-300, AGU, Washington, D.C., 1996.

Galperin, B., and G. L. Mellor, Salinity intrusion and residual circulation in Delaware Bay during the drought of 1984, in *Residual Currents and Long-term Transport, Coastal Estuarine Stud.*, vol. 38, edited by R. T. Cheng, pp. 469-480, AGU, Washington, D.C., 1990.

Godfrey, J. S., A numerical model of the James River Estuary, Virginia, U.S.A., *Estuarine Coastal Mar. Sci., 11*, 295-310, 1980.

Hamrick, J. M., Salinity intrusion and gravitational circulation in partially stratified estuaries, Ph.D. thesis, 451 pp., Univ. of Calif., Berkeley, 1979.

Hansen, D. V., and M. Rattray, Jr., Gravitational circulation in straits and estuaries, *J. Mar. Res., 23*, 104-22, 1965.

Ianniello, J. P., Non-linearly induced residual currents in tidally dominated estuaries, Ph.D. thesis, 250 pp., Univ. of Conn., Storrs, 1977a.

Ianniello, J. P., Tidally induced residual currents in estuaries of constant breadth and depth, *J. Mar. Res., 35*, 755-785, 1977b.

Jay, D. A., and J. D. Smith, Residual circulation in shallow estuaries, 2, Weakly stratified and partially mixed, narrow estuaries, *J. Geophys. Res., 95*, 733-748, 1990.

Kjerfve, B., Bathymetry as an indicator of net circulation in well mixed estuaries, *Limnol. and Oceanogr. 23*, 816-821, 1978.

Kjerfve, B., Circulation and salt flux in a well mixed estuary, in *Physics of Shallow Estuaries and Bays, Coastal Estuarine Stud.*, vol. 16, edited by J. van de Kreeke, pp. 22-29, Springer-Verlag, New York, 1986.

Kjerfve, B., and J. A. Proehl, Velocity variability in a cross-section of a well-mixed estuary, *J. Mar. Res., 37*, 409-418, 1979.

Li, C., Tidally induced residual circulation in estuaries with cross channel bathymetry, Ph.D. thesis, 242 pp., Univ. of Conn., Storrs, 1996.

Li, C., and J. O'Donnell, Tidally induced residual circulation in shallow estuaries with lateral depth variation, *J. Geophys. Res., 102*, 27,915-27,929, 1997.

Li, H., and G. Fang, A vertical coordinate transformation for 3-D numerical modeling of ocean circulation, *Chin. J. Oceanol. Limnol.*, Engl. Edition, *3*, 31-42, 1995.

Linden, P. F., and J. E. Simpson, Modulated mixing and frontogenesis in shallow seas and estuaries, *Cont. Shelf Res., 8*, 1107-1127, 1988.

Lwiza, K. M. M., and B. Connolly, Lateral structure of residual flow and salt distribution in the Lower Hudson Estuary, *J. Geophys. Res.*, in press, 1998.

McCarthy, R. K., A two-dimensional analytical model of density-driven residual currents in tidally dominated, well-mixed estuaries, Ph.D. thesis, 174 pp., Univ. of Del., Newark, 1991.

Nunes, R. A., and G. W. Lennon, Episodic stratification and gravity currents in a marine environment of modulated turbulence, *J. Geophys. Res., 92*, 5465-5480, 1987.

Nunes, R. A., G. W. Lennon, and J. R. de Silva Samarasinghe, The negative role of turbulence in estuarine mass transport, *Estuarine Coastal Shelf Sci., 28*, 361-377, 1989.

O'Donnell, J., Surface fronts in estuaries: a review, *Estuaries, 16*, 12-39, 1993.

Parker, B. B., The relative importance of the various nonlinear mechanisms in a wide range of tidal interactions (review), in *Tidal Hydrodynamics*, edited by B. B. Parker, pp. 237-268, John Wiley, New York, 1991.

Peters, H., Observations of stratified turbulent mixing in an estuary: Neap-to spring variations during high river flow, *Estuarine Coastal Shelf Sci., 45*, 69-88, 1997.

Prandle, D., A. Murray, and R. Johnson, Analyses of flux measurements in the River Mersey, in *Residual Currents and Long-term Transport, Coastal Estuarine Stud.*, vol. 38, edited by R. T. Cheng, pp. 413-430, AGU, Washington, D.C., 1990.

Pritchard, D. W., Salinity distribution and circulation in the Chesapeake estuarine system, *J. Mar. Res., 11*, 106-123, 1952.

Pritchard, D. W., A study of the salt balance in a coastal plain estuary, *J. Mar. Res., 13*, 133-144, 1954.

Pritchard, D. W., The dynamic structure of a coastal plain estuary, *J. Mar. Res., 15*, 33-42, 1956.

Robinson, A. H. W., Ebb-flood channel systems in sandy bays and estuaries, *Geography, 45*, 183-199, 1960.

Robinson, A. H. W., The use of the sea bed drifter in coastal studies with particular reference to the Humber, *Z. Geogr. Suppl., 7*, 1-22, 1965.

Valle-Levinson, A., and K. M. M. Lwiza, The effects of channels and shoals on exchange between the Chesapeake Bay and the adjacent ocean, *J. of Geophy. Res., 100*, 18,551-18,563, 1995.

Valle-Levinson, A., and K. M. M. Lwiza, Bathymetric influences on the lower Chesapeake Bay hydrography, *J. Mar. Syst., 12*, 221-236, 1997.

Valle-Levinson, A., and J. O'Donnell, Tidal interaction with buoyancy-driven flow in a coastal plain estuary, in *Buoyancy Effects on Coastal and Estuarine Dynamics, Coastal Estuarine Stud.*, vol. 53, edited by D. G. Aubrey and C. T. Friedrichs, pp. 265-281, AGU, Washington, D.C., 1996.

Wang, H. V. C., and S.-Y. Chao, Intensification of subtidal surface currents over a deep channel in the Upper Chesapeake Bay, *Estuarine Coastal Shelf Sci., 42*, 771-785, 1996.

Wong, K.-C., On the nature of transverse variability in a coastal plain estuary, *J. Geophys. Res., 99*, 14,209-14,222, 1994.

Zimmerman, J. T. F., Circulation and water exchange near a tidal watershed in the Dutch Wadden Sea, *Neth. J. Sea Res., 8*, 126-138, 1974.

C. Li, Center for Coastal Physical Oceanography, Crittenton Hall, Old Dominion University, Norfolk, VA 23529. (e-mail: chunyan@ccpo.odu.edu)

K. M. M. Lwiza, Marine Sciences Research Center, SUNY at Stony Brook, Stony Brook, NY 11794-5000. (e-mail: kamazima@kafula.msrc.sunysb.edu)

A. Valle-Levinson, Center for Coastal Physical Oceanography, Crittenton Hall, Old Dominion University, Norfolk, VA 23529. (e-mail: arnoldo@ccpo.odu.edu)

K.-C. Wong, College of Marine Studies, University of Delaware, Newark, DE 19716. (e-mail: kuo@chester.cms.udel.edu)

(Received June 23, 1997; revised November 11, 1997; accepted January 27, 1998.)